Hedgehog: Handheld Spherical Pin Array based on a Central Electromagnetic Actuator

Aline Abler[1], Juan Zárate[1], Thomas Langerak[1], Velko Vechev[1] and Otmar Hilliges[1]

***Abstract*— We present Hedgehog, a single-actuator spherical pin-array device that produces cutaneous haptic sensations to the user's palms. Hedgehog can enrich digital experiences by providing dynamic haptic patterns over a spherical surface using a simple, hand-held device. The key to our design is that it uses a single central actuator, a spherical omnidirectional electromagnet, to control the extension of all the 86 movable pins. This keeps our design simple to fabricate and scalable. A core challenge with this type of design is that the pins in the array, made out of permanent magnets, need to have a stable position when retracted. We present a method to compute such an arrays' spatial stability, evaluate our hardware implementation in terms of its output force and pin's extension and compare it against our method's predictions. We also report our findings from three user studies investigating the perceived force and speed of traveling patterns. Finally, we present insights on the possible applications of Hedgehog.**

I. Introduction

Handheld devices are a popular way to interact with virtual content and to receive tactile information [1], [2]. They require minimal instrumentation and offer a familiar interaction paradigm of intuitive handling and exploration of everyday objects [3]. However, such devices rely primarily on vibrotactile actuators that are limited in their ability to stimulate the full range of human mechanoreceptors [4].

Pin array haptic interfaces offer a way to increase the fidelity and localization of haptic feedback on the user's hand. They come in the form of touchable surfaces [5]–[8], wearables [9], [10], and embedded in handheld platforms [11]–[14]. It is desirable to provide varying levels of force intensity as it allows for a larger dynamic range when rendering tactile stimuli. However, this adds mechanical complexity to the system, making the dense pin-array handheld form-factor challenging to achieve.

Instead, we propose a novel way to continuously actuate dense arrays of pins using a single omnidirectional electromagnetic actuator. In such a configuration, the pins are simple passive magnetic elements leveraging the three degrees-of-freedom afforded by the central electromagnet [15]. This allows us to adjust the pin force in a particular activated region dynamically and enables the rendering of various haptic patterns on the device's surface [10], [11]. By using a single actuator with passive actuated elements, we can construct an interface with high pin-density, able to continuously control the force over an affected area, while significantly simplifying the manufacturing and operation of our device compared to traditional pin array interfaces. The use of 3-DoF omnidirectional electromagnets in haptic feedback has been explored previously [15], [16]. However, it should be noted that these examples focus on *graspable* interactions; here we present a *haptic display* based on moving pins.

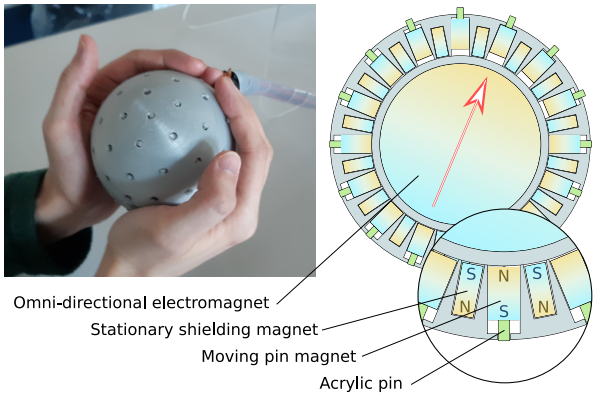

Fig. 1. The Hedgehog Pin Array Haptic Interface, consisting of 86 haptic pins distributed over a 10 cm diameter spherical pin array. A central omni-directional electromagnet repels passive magnets attached to the haptic pins, causing them to push outwards against the user's palms. To stabilize the system, the design contains a number of non-movable shielding magnets.

For the design of such a handheld EM-driven interface, we make the following considerations. As we seek to maximize *pin-density* and *force-output*, we must consider the passive magnet's *arrangement* on the surface, their *size*, and the *cross-talk* magnetic interaction between them. Furthermore, we need to select these factors such that the array is magnetically stable in the "off" position. To this end, we build-up a magnetic model for estimating passive magnetic forces, enabling the design of optimal arrangements and parameter selection. We show that our technique can also accommodate irregularities in such spherical topologies. The model's predicted behavior is shown to be in-line with the fabricated prototype, the pin-array shown in Figure 1. Specifically, we make the following contributions:

- A novel method of evaluating the mutual interaction of passive magnets in non-planar arrays, including a model validation that shows consistent predictions across 4 arrangements, tested experimentally.
- A spherical handheld controller that renders tactile feedback to the user's palms via passive magnetic pins.
- A hardware characterization of the maximum pin force and extension, as well as perceptual studies on the minimum force, force sensitivity, and pattern speed sensitivity.

[1]All authors are with the Department of Computer Science of ETH Zürich, Switzerland. Aline Abler: ablera@student.ethz.ch. Others: first.lastname@inf.ethz.ch

II. Device concept and force modeling

Our haptic interface leverages a single central omni-directional electromagnet (EM) to actuate its pins, which are attached to passive magnets (see Fig.2). All the passive movable magnets face their north pole inwards. The EM is activated such that its north pole points towards a specified direction, represented with a red arrow on Figure 1's schematic. Under activation, the EM repels the magnet at the targeted location, pushing its pin into the user's skin. If the objective is a dynamic pattern, the EM adapts its direction and intensity over time to point to exactly where the stimulus is needed.

We choose a spherical-shell topology as it maximizes the EM's ability to induce force homogeneously in all pins. Since all pin magnets need to be oriented the same way, they repel each other, and the arrangement tends to be unstable. Therefore, we introduce non-moving magnets as shielding oriented in the opposite polarity and interspersed with the pin magnets. If we tune the design correctly, the entire array becomes stable with the pins automatically retracted by default, thus requiring no power. However, while we seek a stable configuration in the off state, we also wish to maximize the overall *pin-density* and the *force-output* of the array when the EM is active. Thus, the pin and shielding magnets' sizes and placement in an chosen arrangement represent a design trade-off. Given that the stability of each magnet depends on the contributions of all its neighbors, we need to consider:

- The EM can induce larger forces in bigger and stronger magnets, but small magnets allow compact designs and denser pin arrays.
- Larger shielding magnets easily retain the pin magnets in their resting position, but the shielding has to be weak enough to be overcome by the electromagnet, whose magnetic force output is limited by overheating.
- A denser pin array provides more contact points for the user; however, it aggravates magnetic *cross-talk* issues due to the closer magnet proximity.

We briefly describe below the essential elements considered to compute each movable pin's induced radial force, how we experimentally validated this model, and its application for optimizing our design.

A. Modeling of the magnetic force interaction

The goal is to determine whether a given magnet arrangement, characterized by the magnets' positions, sizes, and polarities, has a stable resting position. For this, it is necessary to understand the relation between the force[1] F_m induced by all magnets on a test magnet m, and m's vertical offset o. If a stable rest position exists: a) F_m becomes zero at that point; and b) F_m is a restoring force as the magnet is disturbed out of that resting position, meaning that if the displacement is outwards, F_m pushes the magnet back in, and vice versa. If these two conditions are satisfied, the test magnet has a stable resting position.

[1]Only the radial force is of interest, as lateral movement is constrained.

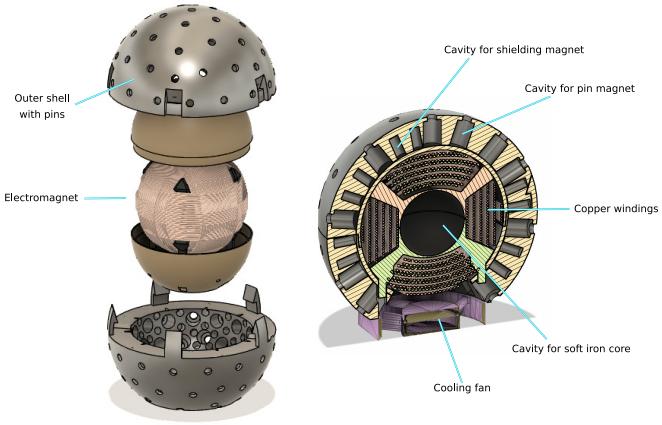

Fig. 2. Exploded view and cross-section of the prototype design. Magnets are inserted from the inside and held in place with a thin hemispherical shell, which in turn encases the electromagnet. The inner shell has a diameter of 70mm. The cavities allow for 0.2mm of tolerance around the magnets.

Our approach to calculate F_m relies on three observations. 1) We can use the principle of magnetic field superposition, as there is no influence of ferromagnetic materials[2]. This allows us to sum up partial magnetic forces between pairs of magnets to obtain an overall result. 2) For any given magnet, most of the other elements within the array are sufficiently far, so the approximation of magnetic dipoles can accurately estimate the magnetic force interaction [17]. The advantage is that the dipole model provides a closed-form solution. 3) For the few remaining magnet pairs that are too close together to use the dipole model, it is feasible to utilize FEA (Finite Element Analysis) simulations.

We leverage the fact that magnet positions are constrained to a sphere surface. We consider the function $f_{s_a,s_b}(\alpha, o)$ that calculates the radial force acting between a pair of passive magnets with sizes s_a and s_b given their relative angle α and the radial offset of the first magnet o. For large α, we utilize the dipole model ($f^{(dip)}$). For small α, we first use a selection of angles α for which we simulate the interaction using FEA. Then, we create a piece-wise linear interpolation of $f^{(fea)}(\alpha, o)$ for each o, from which we can sample an approximate result for any α. In sum, we calculate the force between two magnets in the array with the form,

$$f_{s_a,s_b}(\alpha, o) = \begin{cases} {f^{(fea)}}_{s_a,s_b}(\alpha, o) & \alpha < 30° \\ {f^{(dip)}}_{s_a,s_b}(\alpha, o) & \text{otherwise.} \end{cases} \quad (1)$$

This method allows us to calculate F_m using only a small number of computationally expensive FEA simulations. For this work, we used Comsol Multiphysics with its magnetic modules. The function $f_{s_a,s_b}(\alpha, o)$ is parameterized by the strengths of the magnets a and b, and the size of the sphere.

Knowing the locations of the magnets in an arrangement, we use Eq. 1 to compute the total radial force F_m induced on magnet m by all other magnets in the arrangement M,

[2]We verified with FEA simulations that the EM's core is far enough so that its passive influence in the array becomes negligible.

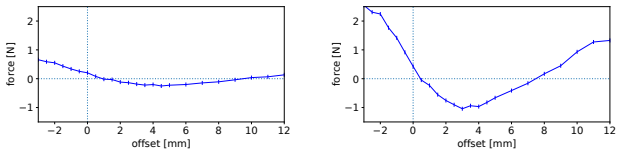

(a) $F_m(o)$ on **cD** (b) $F_m(o)$ on **tkD**

(c) **cD** polyhedron (d) **tkD** polyhedron

Fig. 3. Examples of our approximated function $F_m(o)$ for two different magnet arrangements. Both examples have a stable resting position, as the function crosses zero. For **tkD**, the magnets are in closer proximity, so the slope of the restoring force is more pronounced.

as the magnet m is moved vertically by offset o,

$$F_m(o) = \sum_{m_i \in M \setminus m} f_{s_m, s_{m_i}}(angle(m, m_i), o) * j(m, m_i) \tag{2}$$

with $j(m, m_i)$ checking if the magnets' poles face the sphere equally,

$$j(a, b) = \begin{cases} 1 & \text{if } m_a \text{ and } m_b \text{ have same orientation} \\ -1 & \text{otherwise.} \end{cases} \tag{3}$$

By inspecting the function $F_m(o)$, we can predict whether magnet m has a stable resting position within M and how far it will extend when a given force is applied. Figure 3 shows two examples for specific magnet arrangements. Both arrangements have a zero-force stable position. Also, the curve slopes for offsets in the range 0-2 mm show that the less dense array, named *cD*, would result in softer restoring forces, in opposition to the denser array *tkD*.

The radial force $F_m(o)$ may not be precisely the same for each pin magnet in an array. With our method, we can investigate the behaviour of each individual pin magnet separately. Our method does not make assumptions on the magnets' precise positioning and thus does not require the magnet arrangement to have a strict symmetry. We can thus apply the same method to arrays with irregularities, e.g., with particular locations omitted to make room for a fan mount, a handle, or control electronics. Since the forces at the boundary of such irregularities would be very different from the regular part of an arrangement, we can evaluate whether pins on the border still behave similarly to the remaining ones. In sum, this method allows to efficiently validate the behavior of regular and irregular arrays and find variants in which all pins have a stable resting position and behave similarly when electromagnetic forces are applied.

B. Method validation

To validate our method's generality and accuracy, we tested the interaction force experimentally in different sample arrangements and compared the results to our model. The experiment setup consisted of a 3D-printed rig that holds magnets in a specific arrangement, while a force sensor *(FSAGPNXX1.5LCAC5, Honeywell)* measures the outwards

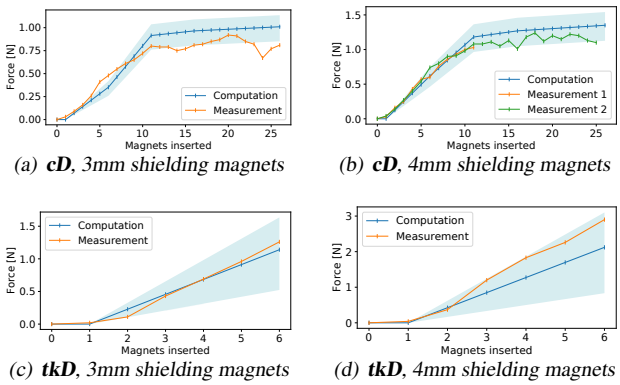

(a) **cD**, 3mm shielding magnets (b) **cD**, 4mm shielding magnets

(c) **tkD**, 3mm shielding magnets (d) **tkD**, 4mm shielding magnets

Fig. 4. Validation of our approximation method through measurements. We measure as well as simulate the radial force $F_m(0)$ as more magnets are inserted into a testing rig. The average accuracy of our model is 81%. This difference can be explained by inaccuracies in the vertical placement of the central magnet in our test setup by approx. ± 0.25 mm, resulting in a range of forces indicated with light blue. In *(b)*, the measurement was interrupted on the first attempt, so a second, equivalent measurement was performed.

pushing force of the central magnet. Neighbor magnets are inserted one-by-one, all with the same polarity, while the sensor records the force value. In Figure 4 we present the result for four different sample arrangements. Our prediction on the force agrees fairly well with the measurements. The normalized root-mean-square deviation for these four experiments is 19% without any need for curve fitting adjustment. Some uncertainties in our experimental setup, such as a vertical offset in the test magnet, may explain the difference.

C. Parameter selection

We choose the magnet's arrangement and the size of the shielding magnets using our force approximation method. To calculate the force which the EM exerts on a movable pin, we follow a similar approach to the one described in [15]. The central 3-DoF EM can provide omnidirectional forces or torques, although we are only interested in the radial component here, inwards and outwards, as all other pin movement are constrained. The pin magnets are chosen to minimize their *size* while maximizing the force that can be induced in them by our EM. We found the best choice to be Neodymium rod magnets with 4 mm in radius and 10 mm in height. All Neodymium magnets used have a remanence of $B_r = 1.35T$.

We choose a hexagonal arrangement for pin and shielding magnets, locating the moving magnets on the center of each face and the shielding magnets on the vertices. We fold the planar hexagons into the spherical shape using icosahedral Goldberg polyhedra [18]. Polyhedra of this class consist of mostly hexagons and few pentagons, which allows for an arrangement with relatively few irregularities. The desired pin density can then be chosen by selecting from topologies with a different number of faces. In Figure 3 we show two examples of such configurations, *cD* and *tkD*. We found the best arrangement of magnets to be one based on the Goldberg polyhedron tkD. It provides the highest magnet density while

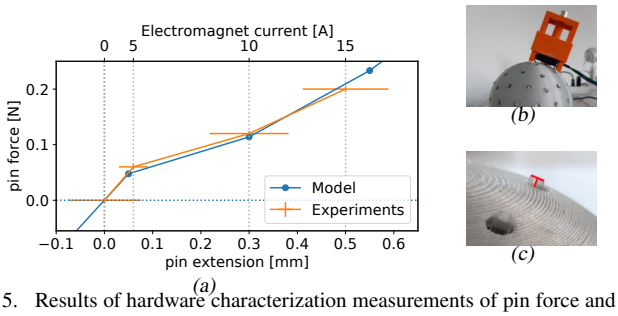

Fig. 5. Results of hardware characterization measurements of pin force and extension, including comparison to calculated results from our method (section II). The modeled relation between force and pin extension corresponds well to our measurements.

still having a stable resting position, as validated by our method. The shielding magnets have a radius of 2 mm, as smaller magnets are not able to retain the pin magnets according to our method.

III. Hardware Implementation & Tests

For the array's fabrication, we embedded the pin and shielding magnets in a plastic casing that only allows the pin magnets to move vertically (see Figure 1). Haptic pins made of cut acrylic push the user's skin when their respective magnet is actuated. In Figure 2 we present an exploded view of our device. Of the 86 pins on the final design, the average human hand covers approximately 30.

In terms of the EM itself, our prototype implementation reuses the three-axis electromagnet from Omni [15] as its central actuator. It also inherits Omni's cooling system and control electronics. The device can be operated indefinitely at 5 A of actuation, and excursions up to 15 A (maximum current) are possible for periods of 30 seconds. For details on the EM actuator please refer to [15].

A. Pin's force and extension

The maximum force and displacement of the individual pins are two of the main physical characteristics that define our device's haptic capabilities. The former can be measured at zero displacement, the latter at zero load, and we describe each of these tests below. To determine the maximum force a pin exerts, we mounted a force sensor (see Section II-B) on top of one of the pins as shown in Figure 5(b). We measure the force for EM actuation currents varying from 0 A to 10 A. As the EM's field increases linearly with the current, so does the induced force in the magnet. We found for our specific hardware configuration a force-to-current ratio of 12.6 $\frac{mN}{A}$, corresponding to 200 mN at maximum actuation. The pin extension without load was measured using photographs (see Figure 5(c)). We average multiple photos for each of the actuation values tested: 5, 10 and 15 A. Results for pin extension and force are combined in a single plot in Figure 5. The experimental results are compared with the calculated forces from subsection II-A, showing an excellent agreement between our model and the experiments. Given the slope in Figure 5 and the magnet mass (4 gr) we obtain 50 Hz for the resonant frequency: below it the pins respond following the EM actuation.

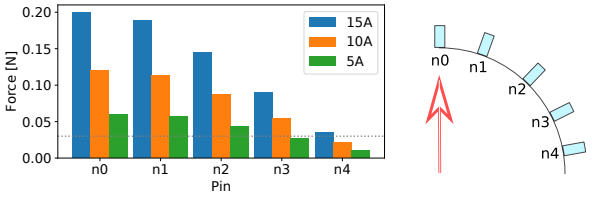

Fig. 6. Activation spread for the neighbors of target pin (n0) at different activation currents. As, according to our user study in section IV, users can only feel forces stronger than 30 mN (dotted line), pins with force values below that can be considered deactivated.

B. Activation spread

As we use a single central EM to operate all pins, this configuration does not allow us to actuate a single pin in isolation. Even if the magnetic field is pointed at a specific pin, neighboring pins will react to this actuation, albeit less strongly. As a result, there is always an area of activated pins. The activation of a neighbor pin increases with higher actuation currents but decays with the cosine of the angle between that neighbor and the target location. Figure 6 shows the activation spread for various levels of current and neighbor angular positions.

IV. User Evaluation

We test our device's different perceptual characteristics, mainly in terms of force and speed, to give a context of the interaction possibilities that it allows. For this purpose, we designed a three-part user study to answer the following research questions regarding our prototype:

A) What is the minimum force users can perceive?
B) What is the force sensitivity of users in terms of JND (just noticeable difference)?
C) What is the pattern speed sensitivity of users in terms of JND?

The measured results inform our application design and allow for a comparison between our device and similar work.

Overall Procedure

We recruited 10 participants (3 female) aged 22 to 55 to perform the three tests. For all experiments, users were asked to place their dominant hand on top of the device, which would play a dynamic circular pattern (Figure 7). Participants were required to wear noise-canceling headphones to mask the small sound emitted by the prototype.

Each part of the user study consisted of a number of blocks. We use a two-up-one-down weighted adaptive staircase procedure [19] to determine the intensity level at which a user has an 80% probability of detecting device activation (Experiment A) or correctly identifying the test stimulus (Experiments B and C). The parameters for each experiment are given in Table I. The test parameter D is set to the initial value D_i in the first block. D is increased by the step size ΔD after each negative or incorrect response, and decreased by $0.5488 * \Delta D$ after two consecutive positive or correct responses. After the first R_1 reversals, ΔD is halved, and after the next R_2 reversals, it is halved again. The experiment

Experiment	Reference level	D_i	ΔD	R_1	R_2	R_3
A	N/A	5A	1A	5	5	5
B	5A (63 mN)	100%	20%	3	3	4
C	10 pin/s	100%	40%	3	3	4

TABLE I

PARAMETERS FOR THE WEIGHTED ADAPTIVE STAIRCASE PROCEDURE.

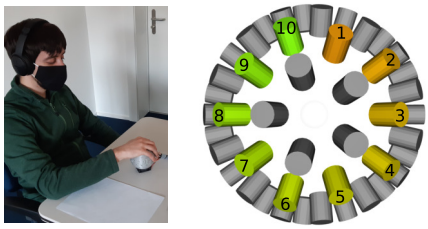

Fig. 7. JND study setup and schematic of the circular pattern used. The schematic shows the positions of pin magnets, seen from above. Pins 1-10 are activated sequentially by the electromagnet in the depicted order.

terminates after R_3 more reversals with the final ΔD. The average of all but the first two reversal points is calculated for each participant.

A. Minimum Force Threshold

Method: Each experiment block contains one trial, during which the device is activated, playing the dynamic circular pattern for five seconds at a speed of 10 pin/s using the test force D. Participants were told that during some trials, the device might not activate at all. Participants had to indicate whether they thought the device had been activated. *Results:* As a primary finding, participants could sense activation forces as low as 30 mN (i.e., an actuation current of 2.1 A), which gives a lower bound for perceivable force.

B. JND of Force

Method: Each experiment block contains two trials each. During each trial, the device is activated, playing a dynamic circular pattern for five seconds at a speed of 10 pin/s. One trial plays the reference stimulus, the other does the test stimulus, in which the activation force is increased w.r.t. the reference stimulus by a force difference D. The trials within a block were randomly ordered, and participants had to indicate which trial used a stronger activation force. *Results:* Participants were able to distinguish force differences of 13% on average, which at the reference stimulus corresponds to a difference of 8 mN. We estimate that it should be possible for users to distinguish roughly ten different levels of force within the device's operational range.

C. JND of Speed

Method: Analogous to Part B, but the test stimulus differs from the reference stimulus in pattern speed. Participants were asked to identify the trial using a faster speed. The activation force is constant across trials at 63 mN (or 5 A of actuation), this being the highest level of indefinitely sustainable force output without overheating. *Results:* Participants were able to distinguish pattern speed differences of 47% on average. Overall, it was harder for participants

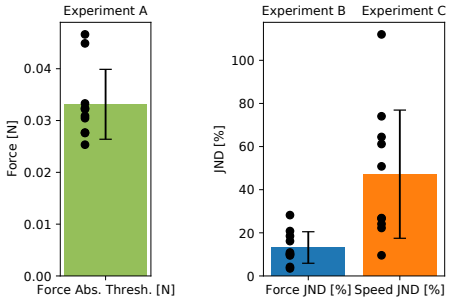

Fig. 8. JND study results. Individual averages are indicated as black dots. The bars denote the average of averages, and the error bars denote the standard deviation. JND results are given in percent of the reference level (the Weber fraction).

Fig. 9. A user enjoying the racing game demo. Directional haptic feedback is given when the car crashes into an obstacle to inform the user where the crash occurred (relative to the car). The pin force scales with the impact velocity.

to determine speed differences than the force's JND. For example, one participant reported that they perceived the slower patterns as smooth circles, while the faster ones seemed more "random". The exhibited JND allows for several levels of speed rendering, and its possible that other patterns may exhibit different levels of sensitivity [10].

V. APPLICATIONS

To explore our haptic device's usage as a handheld controller, we integrated a wireless IMU sensor (*Xsens MTw Awinda*) and connected it as a controller for a racing game. Our device can improve upon vibrotactile actuation by indicating a collision event together with the localization of where it occurred. We performed an informal tryout session of this application with two participants, after which we recorded their feedback (Figure 9). Participants thought the haptic feedback added by our prototype improves immersion. They were particularly impressed by feedback when the car flipped upside down and tumbled after some daring maneuvers.

We have also built a basic application to test our device in a constant-use setting, in which the pins are actuated in the upwards direction as the user rotates the device freely. Such a mechanism could be useful in a navigation task for the visually impaired, with the device pointing in a desired direction. We found that at the device's peak force output of 200 mN, the direction is easier to distinguish than at the continuously sustainable 63 mN.

VI. Discussion and Conclusion

We presented a handheld, spherical haptic display based on passive moving magnets and a single central electromagnetic actuator. To explore the array's spatial design, we leveraged a model to predict its mechanical behavior with a sufficient degree of accuracy. We used this approach to build a 10 cm diameter prototype with 86 active pins. In terms of the *force-displacement* of output our device, the tests confirm what we found using our model: up to 200 mN of haptic force at max load or 0.5 mm displacement with zero-load (see Figure 5).

As shown in our user study, these numbers resulted in a relatively large dynamic range for users to perceive, allowing us to render up to 10 distinguishable levels of force. We found a lower bound of 30 mN for perceptible force. It is important to note that bi-stable pin-array designs such as those used in [9], [10], and in general, devices that cannot render varying levels of force, would miss out on the rich, dynamic range perceived by users. While we did not conduct a direct study on *localization* on the surface, the high pattern-speed JND showed that the device output is limited in this respect. The maximum extension of a single pin (0.5 mm) would seem sufficient in communicating a pin location. However, one limitation of our approach is that nearby pins would also be activated (See Fig. 6), possibly reducing users' sensitivity in speed discrimination. Activation spread could be addressed in future works, for example, by using electrostatic friction [7], [20] to individually break passive pins by surrounding them with a dielectric material.

In terms of *pin-density*, we found that despite stronger magnetic interactions, dense arrays are suitable for our actuation mechanism. We achieved a stable configuration based on the *tkD* polyhedron, which is the densest within the Goldberg polyhedra class for our sphere size. Arrangements based on other polyhedra (e.g., quad spheres) are conceivable and might achieve a yet higher pin density. Our magnetic force approximation method can be used to judge different arrangements' suitability, both regular and irregular. The technique can be used for different sphere sizes and could be generalized to other shapes of passive magnet arrays. While small enough to be picked up and used as a handheld device, our current implementation's 1.2 kg weight means that it has to be held with both hands. A stronger electromagnet with a more efficient cooling system could achieve the same device performance with a smaller weight and form factor or produce larger forces keeping the current form factor.

Finally, the device's ability to dynamically adjust pin force adds an essential dimension to the haptic feedback, allowing us to convey a measure of intensity more intuitively. Our demo applications exemplify potential use cases for haptic display interfaces driven by a single central actuator. It will also be interesting to combine our haptic display with other input forms, such as buttons, triggers or 6-DOF tracking.

ACKNOWLEDGMENT

This work was supported in part by grants from the Hasler Foundation (Switzerland) and ERC (OPTINT StG-2016-717054).

References

[1] Sony, "DualSense," https://www.playstation.com/en-us/accessories/dualsense-wireless-controller/, accessed: 16.02.2021.

[2] HTC Vive, "Controller," https://www.vive.com/us/accessory/controller/, accessed: 16.02.2021.

[3] R. L. Klatzky, S. J. Lederman, and V. A. Metzger, "Identifying objects by touch: An "expert system"," *Perception & psychophysics*, vol. 37, no. 4, pp. 299–302, 1985.

[4] R. S. Johansson and J. R. Flanagan, "Coding and use of tactile signals from the fingertips in object manipulation tasks," *Nature Reviews Neuroscience*, vol. 10, no. 5, p. 345, 2009.

[5] D. Leithinger, S. Follmer, A. Olwal, and H. Ishii, "Physical telepresence: shape capture and display for embodied, computer-mediated remote collaboration," in *Proceedings of the 27th annual ACM symposium on User interface software and technology*, 2014, pp. 461–470.

[6] J. Jung, E. Youn, and G. Lee, *PinPad: Touchpad Interaction with Fast and High-Resolution Tactile Output*. New York, NY, USA: Association for Computing Machinery, 2017, p. 2416–2425. [Online]. Available: https://doi.org/10.1145/3025453.3025971

[7] K. Zhang, E. J. Gonzalez, J. Guo, and S. Follmer, "Design and analysis of high-resolution electrostatic adhesive brakes towards static refreshable 2.5d tactile shape display," *EEE Trans. Haptics*, vol. 12, no. 4, p. 470–482, Oct. 2019. [Online]. Available: https://doi.org/10.1109/TOH.2019.2940219

[8] Y. Ujitoko, T. Taniguchi, S. Sakurai, and K. Hirota, "Development of finger-mounted high-density pin-array haptic display," *IEEE Access*, vol. 8, pp. 145 107–145 114, 2020.

[9] F. Pece, J. J. Zarate, V. Vechev, N. Besse, O. Gudozhnik, H. Shea, and O. Hilliges, "Magtics: Flexible and thin form factor magnetic actuators for dynamic and wearable haptic feedback," in *Proceedings of the 30th annual ACM symposium on User interface software and technology*, 2017, pp. 143–154.

[10] V. Vechev, J. Zarate, D. Lindlbauer, R. Hinchet, H. Shea, and O. Hilliges, "Tactiles: Dual-mode low-power electromagnetic actuators for rendering continuous contact and spatial haptic patterns in vr," in *2019 IEEE Conference on Virtual Reality and 3D User Interfaces (VR)*. IEEE, 2019, pp. 312–320.

[11] H. Benko, C. Holz, M. Sinclair, and E. Ofek, "Normaltouch and texturetouch: High-fidelity 3d haptic shape rendering on handheld virtual reality controllers," in *Proceedings of the 29th Annual Symposium on User Interface Software and Technology*, 2016, pp. 717–728.

[12] S. Yoshida, Y. Sun, and H. Kuzuoka, "Pocopo: Handheld pin-based shape display for haptic rendering in virtual reality," in *Proceedings of the 2020 CHI Conference on Human Factors in Computing Systems*, ser. CHI '20. New York, NY, USA: Association for Computing Machinery, 2020, p. 1–13. [Online]. Available: https://doi.org/10.1145/3313831.3376358

[13] D. K. Chen, J.-B. Chossat, and P. B. Shull, "Haptivec: Presenting haptic feedback vectors in handheld controllers using embedded tactile pin arrays," in *Proceedings of the 2019 CHI Conference on Human Factors in Computing Systems*, 2019, pp. 1–11.

[14] E. Strasnick, J. Yang, K. Tanner, A. Olwal, and S. Follmer, "shiftio: Reconfigurable tactile elements for dynamic affordances and mobile interaction," in *Proceedings of the 2017 CHI Conference on Human Factors in Computing Systems*, 2017, pp. 5075–5086.

[15] T. Langerak, J. J. Zárate, D. Lindlbauer, C. Holz, and O. Hilliges, "Omni: Volumetric sensing and actuation of passive magnetic tools for dynamic haptic feedback," in *Proceedings of the 33rd Annual ACM Symposium on User Interface Software and Technology*, 2020, pp. 594–606.

[16] R. Zhang, T. J. Schwehr, and J. J. Abbott, "Dimensional reduction for 6d vibrotactile display," *IEEE Transactions on Haptics*, vol. 13, no. 1, pp. 102–108, 2020.

[17] K. W. Yung, P. B. Landecker, and D. D. Villani, "An analytic solution for the force between two magnetic dipoles," *Magnetic and electrical Separation*, vol. 9, 1970.

[18] J. H. Conway, H. Burgiel, and C. Goodman-Strauss, *The symmetries of things*. CRC Press, 2016.

[19] M. A. Garcıa-Pérez, "Forced-choice staircases with fixed step sizes: asymptotic and small-sample properties," *Vision research*, vol. 38, no. 12, pp. 1861–1881, 1998.

[20] R. Hinchet, V. Vechev, H. Shea, and O. Hilliges, "Dextres: Wearable haptic feedback for grasping in vr via a thin form-factor electrostatic brake," in *Proceedings of the 31st Annual ACM Symposium on User Interface Software and Technology*, 2018, pp. 901–912.